From Well-Entangled to Partially-Entangled Wormlike Micelles: A Characterization by Rheological Modeling, Diffusing Wave Spectroscopy, and Small-Angle Neutron Scattering

Journal:	*Soft Matter*
Manuscript ID	SM-ART-10-2018-002223.R1
Article Type:	Paper
Date Submitted by the Author:	05-Dec-2018
Complete List of Authors:	Zou, Weizhong; University of Michigan, Chemical Engineering Tan, Grace; University of Michigan, Chemical Engineering Jiang, Hanqiu; University of Cincinnati, Department of Chemical and Materials Engineering Vogtt, Karsten; University of Cincinnati, Department of Chemical and Materials Engineering Weaver, Michael; P&G, Analytical Sciences Koenig, Peter; The Procter & Gamble Company Beaucage, Gregory; University of Cincinnati, Biomedical, Chemical, and Environmental Engineering Larson, Ronald; University of Michigan, Chemical Engineering

SCHOLARONE™
Manuscripts

From Well-Entangled to Partially-Entangled Wormlike Micelles: A Characterization by Rheological Modeling, Diffusing Wave Spectroscopy, and Small-Angle Neutron Scattering

Weizhong Zou[#], Grace Tan[#], Hanqiu Jiang[‡], Karsen Vogtt[‡], Michael Weaver[+], Peter Koenig[+], Gregory Beaucage[‡], and Ronald G. Larson[#]*

Chemical Engineering, University of Michigan, Ann Arbor, MI 48109

‡ Biomedical, Chemical, and Environmental Engineering, University of Cincinnati, Cincinnati, OH 45221

+ The Procter & Gamble Company, Mason, OH 45040

*Correspondence: email: *rlarson@umich.edu*, phone: (734) 936-0772, FAX: (734) 763-0459

Abstract

We combine mechanical rheometry, diffusing wave spectroscopy (DWS), and small angle neutron scattering (SANS) with a simulation model, the "pointer algorithm," to obtain characteristic lengths and time constants for wormlike micelle (WLM) solutions over a range of salt concentrations encompassing the transition from unentangled to entangled solutions. The solutions contain sodium lauryl sulfate (SLE1S), cocoamidopropyl betaine (CAPB), and NaCl. The pointer algorithm is extended to include relaxation of unentangled micelles, allowing micelle parameters to be extracted from the rheology of partially entangled solutions. DWS provides the data at high frequency needed to determine micelle persistence length accurately. From pointer algorithm fits to rheology, we observe a salt-induced rapid change in micellar length as the solution enters the well-entangled regime and a weaker growth with surfactant concentration consistent with mean-field theory. At a lower surfactant concentration, micelle lengths and persistence length from SANS are roughly consistent with values from rheology once the lower surfactant concentration used in SANS is accounted for. This is, to our knowledge, the first time that quantitative comparisons of structural features including micelle length are made between rheology and SANS. Finally, scaling laws for micelle diffusion and recombination times indicate that micelle kinetics are reaction controlled leading to mean-field recombination with surrounding micelles over the entire range of concentration of interest except at very low and very high surfactant concentrations where either short micelles or branched micelle clusters are dominant.

1. Introduction

Surfactant micelles, known for their multiple self-assembled structures and flow behaviors, have been extensively used as carriers of drug molecules,[1] templates,[2] solubilizers,[3] extractants,[4] and rheology modifiers,[5] either as mixtures or as individual components. Given the ease of tuning the non-covalent interactions between surfactant molecules, a wide range of micellar morphologies, such as ellipsoids, worms, vesicles, lamellae, and others can be achieved through the addition of simple electrolytes, cosurfactants, or strongly binding counterions (so-called hydrotropes) into the solutions.[6-8] Such mixed surfactant solutions sometimes exhibit prominent gains in viscoelasticity associated with the formation of large surfactant aggregates, and, in particular, formation of transient networks of entangled wormlike micelles (WLMs), which are commonly encountered in detergent-using industries.[9-11] The formation of these long WLMs is attributed to specific molecular packing, leading to spontaneous preferred curvature of the micelle surfaces, promoting the cylindrical shape.[9,12] Because of the various ways the additives can tailor the micellar surface curvature, for instance, through electrostatic screening, hydrophobic binding, etc.,[13-16] there exist great opportunities for improved properties through the synthesis of new functional materials: for example, recent years have witnessed a growing interest in changes of flow properties of WLM solutions through the addition of stimuli-responsive small molecules.[17-19]

Besides the fundamental interest in controlling the microstructure of surfactant assemblies, intense efforts have been made over decades to better understand the coupling between microstructure and the rheological properties of WLM solutions. As directly visualized by cryo-TEM,[20,21] WLMs assembled from small-molecule surfactants have a diameter of 3-5 nm while their contour length can reach a few micrometers in the semi-dilute regime giving rise to the

occurrence of entanglements and eventually an enhanced viscoelasticity.[16,22] In this regard, WLMs are similar to polymers except that they are subject to constant breaking and re-forming in thermal equilibrium with their surfactant "monomers",[23,24] which prevent permanent mechanical degradation of the worms, making them desirable candidates as heat-transfer fluids and fracturing liquids that are subject to large stresses.[25] However, when the applied flow rate is high enough to disturb the equilibrium WLM structures, which in turn modifies the flow, a rich variety of nonlinear rheological features can appear, including heterogeneous shear bands and flow-induced phase separation.[26,27]

Thus, to unveil basic property-structure relationships behind different flow behaviors of WLMs, methods that allow monitoring of the dynamics of micelles are needed. Fortunately, micelle characterization has benefited from an increasing number of advanced techniques, including ultrasonic velocimetry,[26] and micro-cantilevers,[28] in addition to more conventional flow birefringence, and light and neutron scattering. However, quantitative estimates from those methods of characteristic micellar length and time scales still remains challenging. The difficulties, to a large extent, arise from limitations in length scales, time scales, or concentrations that can be probed by these methods. Since the rheology of WLM solutions appears to be rather sensitive to subtle changes in either length scales or lifetimes of the microstructures, an appropriate model of micelle rheology can offer an indispensable assistance in inferring micelle properties. For entangled WLM solutions, as confirmed by Cates in his well-recognized theory, micellar properties such as their length and breakage and reformation times can be deduced from the linear rheological responses, namely, the storage (G') and the loss (G") modulus.[29-31]

However, when the surfactant concentration is low, some of the micelles are too short to form entanglements. Unlike the well-entangled long WLMs, these short micelle rods relax much faster and therefore contribute less to the viscosity than do entangled micelles. Without modification, the Cates theory is inapplicable for capturing the rheological behaviors for solutions with significant numbers of unentangled micelles. On the other hand, while scattering techniques can extract length scales of unentangled micelles, these methods do not readily yield the lengths of partially or fully entangled micelles. Thus, there is a gap in characterization methodology between the dilute concentrations for which scattering techniques can extract micelle parameters, and the semi-dilute ones for which rheology and rheological theory allows determination of micelle parameters. This gap is here addressed by extending our recently developed "pointer" simulation model[32,33] to account for the contributions from unentangled micelle rods to the overall rheology. In what follows, the original simulation model is briefly reviewed with adjustments added to allow its application to partially entangled WLM solutions. Since macro-rheology by itself is insufficient to indicate the local structure, diffusing wave spectroscopy (DWS) is also employed in order to fully characterize WLMs over six decades of oscillation frequency. A number of important physical phenomena for WLMs are explored, including the relaxation mechanisms of unentangled micelles, the effect of the salt-induced increase in entanglements on linear rheology, and the possibility of micellar self-recombination. In addition, a comparison is provided between micellar parameters estimated from rheology and those obtained from SANS, and suggestions for how the gap in concentrations separating them can be bridged by scaling laws.

2. Experimental Section

Materials. The surfactant solutions contain two types of surfactants, "SLE1S" and "CAPB", along with a simple salt (sodium chloride, NaCl). SLE1S (Scheme 1a) is an abbreviation for commercial SLES (sodium lauryl ethylene glycol sulfate, industrial grade) with one ethoxyl group (EO) on average (but with a distribution of the number of EOs ranging from 0 to 10); and CAPB (Scheme 1b, cocamidopropyl betaine, industrial grade) is a zwitterionic co-surfactant. The weight ratio of SLE1S/CAPB in the solution is fixed at 8.57. The activity of the SLE1S paste was verified using potentiometric anionic surfactant titration, ASTM D4251. D_2O (99-96%, analytical grade, from Cambridge Isotrope Laboratories, Inc.) was used as the solvent of WLM solutions to facilitate the comparison of characterized micellar properties from rheology and from small angle neutron scattering (SANS). Because of the complexity of these materials, the weight percentage (wt. %), instead of the molar concentration, is generally chosen to represent the composition. Samples were prepared by mixing the above individual components in the following order: concentrated surfactant paste, D_2O, bead solution, and salt solution (20 wt. % in D_2O, analytical grade). All the samples were then well mixed at ratios designed to produce the desired surfactant and salt concentrations (reported below) and allowed to rest overnight for degassing prior to measurements.
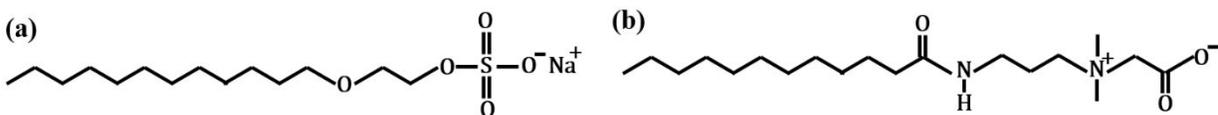
Scheme 1. The chemical structure for (a) SLE1S, and (b) CAPB.

Macro-rheology. An MCR-702 TwinDrive rheometer (Anton Paar) equipped with a 50mm steel, 0.5° cone and plate, was used for measurements. The zero shear viscosity was measured in

a flow experiment, typically over the range of 0.01-0.1 s^{-1}, where a low shear viscosity plateau was observed. The frequency sweep measurements were conducted with logarithmic variation in the applied strain amplitude through a built-in "RheoCompass" software, which allows for a TrueStrain® criteria to ensure that the specified strain amplitude is achieved at each frequency. Such a variation in the strain amplitude maximizes the torque signal at lower frequencies while minimizing the effects of inertia at high frequencies within the linear viscoelastic range of the samples. For example, at a frequency of 0.1 rad/s, the strain amplitude was 13%, and then decreased logarithmically to 0.2% as frequency increased to 600 rad/s. The counter-rotation mode was also used to divide the total strain amplitude between the upper and lower drive which helps limit inertial effects at high frequencies. The geometry was inertially corrected prior to measurement, and the air bearing was mapped and coded in precision mode as prescribed in the RheoCompass software. Only data where the measured torque deviates from the lower-drive-electric torque by < 2% were included (which is the recommended criterion by Anton-Paar), and data points with abrupt changes in moduli were also rejected. For the low viscosity samples, the above criteria usually limited the frequency spectrum to 10–100 rad/s. We sampled 10 data points per decade of frequency to obtain enough information in a reasonable time. Samples were freshly loaded each time and a solvent trap was used to prevent solvent evaporation near the edge. All rheological measurements were performed within the linear viscoelastic regime at 25 °C unless otherwise specified. Each sample was re-measured and the standard deviation of each rheological measurement was found to be less than 5%.

DWS. As an optical micro-rheology approach, diffusing wave spectroscopy (DWS) was also applied to observe the high-frequency behavior (10−10^5 rad/s) of WLM solutions. Details about

DWS can be found in references.[34,35] The wavelength of light used in the DWS was 532 nm. Solutions of sulfate latex particles (8.2 wt. %, analytical grade, from Life Technology) with a bead size of 600 nm were used as molecular probes with final bead concentration at 0.5 wt. %. These beads, made of IDC polystyrene latex with a hydrophobic surface, were stabilized with a low level of sulfate charges (thus rendering the beads negatively charged), and were surfactant free. The samples for DWS measurement were well mixed with 0.5 wt % beads before adding 10 wt % NaCl solutions to avoid shocking of the samples. A high-speed vortex mixer was also used to ensure the homogeneity of the samples. Thus, it is reasonable to believe the quantity of the surfactants absorbed to the surface of the particles, if any, would be negligible in comparison to the total surfactant concentration. After 12 h of equilibration, scattering from the sample was measured in a 5 mm glass cell on an LS Instruments RheoLab 7.1.0 system. The transport mean free path l^* (=552 μm) was determined from the control sample with the same-size beads in water.

SANS. Neutron scattering was performed with the GP-SANS instrument at Oak Ridge National Laboratory in Tennessee, USA. The measured data were reduced using a plugin for the Igor Pro software provided by the instrument scientists. For the background subtraction, the scattering intensity $I(q)$ of the pure D_2O/NaCl solution was employed. $I(q)$ is considered to be a unified combination of individual scattering contributions $I_1(q)$ and $I_2(q)$ from the cylindrical subunits and the large-scale structure of these units, respectively. The volume fraction times contrast squared $\phi \cdot \Delta \rho^2$ and the radius R_1 and length L_1 of the cylindrical subunits constituting the wormlike chain were obtained by fitting to the experimental data. R_1 is treated as a polydisperse variable with the corresponding geometric standard deviation or dimensionless width parameter given by $\sigma_{R,1}$. Fits were performed using the Igor Pro software with a user-programmed algorithm

function for $I(q)$ and a built-in function for the linear regression. For values of parameters derived from the fits, error bars were also calculated according to the propagation of error using the standard deviations. The detailed wormlike chain model and fitting procedure for SANS are described in references.[36,37]

3. Modeling and Simulation

The Cates theory has been a notable success in explaining the linear rheology of entangled WLMs, especially the single Maxwellian relaxation behavior observed for long micelles and short micelle breakage times. The theory, however, leaves out the effects of micelle rigidity (i.e., bending modes and tight entanglements), the contributions of unentangled micelles, entanglement constraint-release dynamics, and micelle branches, which limits its ability to explain the full range of WLM rheology across the range of surfactant concentrations, temperatures, salt concentrations, and presence of additives.[10,12,24,27,28,38,39] However, although other models and simulations in this area exist,[16,40-43] the conceptual framework provided by the Cates theory remains highly attractive, and when supplemented with some additional physics, we believe, can be used for quantitative estimation of micellar properties from linear rheology, some of which are difficult to measure in any other way, except under very restricted conditions. To include the additional physics, we have developed a novel mesoscale simulation model for well entangled WLMs, in which "pointers" are used to track the unrelaxed portions of WLMs, as they diffuse within their entanglement tubes, by reptation and primitive path fluctuations, accelerated by the creation of new micelle chain ends through micelle breakage.[32,33] A modified "Genetic Computer Algorithm," which mimics biological evolution, was also incorporated into the model to transform the simulation results from the time to the frequency domain, thereby allowing direct comparison of model predictions to

experimental G' and G'' data.[32] A recent application of this simulation model to commercial surfactant solutions[44] yielded predictions of average micelle length $\langle L \rangle$:1~3 μm; mesh size ξ:80~100 nm; persistence length l_p:60~70 nm; and breakage time $\bar{\tau}_{br}$ (which is also the fusion time for micelles at thermal equilibrium):0.05~0.15 s. These values are in ranges generally consistent with those reported previously for other entangled worm-like micellar surfactant solutions in the literature; i.e., ~0.1 $-$ 1 μm for $\langle L \rangle$,[25,31] 50~100 nm for ξ,[45] 30~125 nm for l_p,[10] 0.01~0.1 s for $\bar{\tau}_{br}$.[46]

To extend the above success in modeling unbranched but well-entangled WLMs to the whole range of surfactant and salt concentrations, additional relaxation dynamics, besides those have already included in the original Pointer Algorithm,[32] are needed, especially to account for the effects of unentangled micelles and of micelle branches. The former are usually present in significant concentration at low surfactant or salt concentrations, where aggregates with large surface curvature are energetically less disfavored, leading to a low end-cap energy and short micelles. Orientational and positional diffusion of these unentangled semi-flexible "rods" is not restricted by an entanglement tube, so that the stress imposed on them can be relaxed relatively quickly by unrestricted rotation. We have therefore incorporated unimpeded rotary relaxation of short micelles into our Pointer Algorithm, giving predictions of their contributions to rheology described by Eqs. 1 and 2,[47] which enables both characterization of WLM solutions at low surfactant or salt concentration, and comparison with micellar parameters derived from SANS as discussed later:

$$G'(\omega) = \sum_i G_i \frac{(\omega/D_{r,i})^2}{1+(\omega/D_{r,i})^2}, \quad G''(\omega) = \sum_i G_i \frac{(\omega/D_{r,i})}{1+(\omega/D_{r,i})^2} \tag{1a}$$

$$D_{r,i} = \frac{3k_BT}{\pi\eta_sL_i^3}[ln(L_i/d)-0.8], \quad G_i = \nu(L_i)k_BT \tag{1b}$$

In the above equations, G_i and $D_{r,i}$ are, respectively, the modulus and the rotary diffusivity for WLMs with length of L_i, k_B is the Boltzmann constant, T is the temperature, η_s is the solvent viscosity, and d is the micelle diameter. $\nu(L_i)$ is the number density of micelles with length of L_i. Note that Eq. 1 is only applicable to micelles with length smaller than the entanglement length l_e. Rouse and bending modes are added using the following equations:

$$\begin{cases} G'(\omega) = \sum_i G_i \sum_{p=1}^{N_{K,i}} \frac{(\omega\tau_{R,i}/2p^2)^2}{1+(\omega\tau_{R,i}/2p^2)^2} \\ G''(\omega) = \sum_i G_i \sum_{p=1}^{N_{K,i}} \frac{(\omega\tau_{R,i}/2p^2)}{1+(\omega\tau_{R,i}/2p^2)^2} \end{cases}, \quad \tau_{R,i} = \frac{4\eta_sL_i^2l_p}{3\pi k_BTln(L_i/d)}, \quad \text{for } l_p < L_i < l_e \tag{2a}$$

$$G^*(\omega) = \frac{\rho}{15}\frac{2^{3/4}k_BT}{l_p}(i\omega\tau_p)^{3/4} + i\omega\eta_s, \quad \rho = \frac{4\phi}{\pi d^2}, \quad \tau_p = \begin{cases} \frac{\zeta_\perp L_i^4}{k_BTl_p}, & \text{for } L_i < l_p \\ \frac{\zeta_\perp l_p^3}{k_BT}, & \text{for } L_i \geq l_p \end{cases} \tag{2b}$$

Here Eq. 2a is the standard formula for Rouse relaxation, with the longest *orientational* Rouse time $\tau_{R,i}$ of species i differing by a factor of two from the Rouse stress relaxation time, which is accounted for by the factor of two multiplying p^2 in Eq. 2a. $N_{K,i}$ is the number of Kuhn steps in species i, which is given by the length of the micelle divided by twice the persistence length. Eq.

2b accounts for the high frequency bending motions, with the characteristic time τ_p for both short micelle rods ($L_i < l_p$) and long worms ($L_i \geq l_p$). ρ is the micelle contour length per unit volume, ϕ is the surfactant volume fraction, and $\zeta_\perp$ is the perpendicular drag coefficient for bending motions. These formulas were also presented in our previous work.[32]

Because of the polydispersity in micelle length distribution, it is reasonable to believe that there always exists a certain fraction of micelles which remain unentangled ($L_i < l_e$) with their effects on the solution viscoelasticity being of importance even in the semi-dilute regime.[72] Depending on the ratio of $\langle L \rangle$ to l_e, i.e., the average entanglement number per micelle $\overline{Z} \equiv \langle L \rangle / l_e$, the percentage of entangled vs unentangled WLMs varies, and the micelles within these two subpopulations would experience distinct relaxation mechanisms as illustrated in Table 1.

Table 1. A comparative list of relaxation mechanisms and the associated characteristic times for entangled and unentangled micelles

Range of length scales	Unentangled		Range of length scales	Entangled
	$L_i < l_p < l_e$	$l_p < L_i < l_e$		
d to l_p	Bending motion with τ_p (L_i,l_p) (Eq. 2b)	Bending motion with $\tau_p(l_p)$ (Eq. 2b)	d to l_p	Bending motion with $\tau_p(L_i,l_p)$ (Eq. 2b)
l_p to L_i	No Rouse motion	Rouse motion with $\tau_R(L_i)/p^2$ (Eq. 2a)	l_p to l_e	Local Rouse motion with $\tau_R(L_i)/p^2$
L_i	Rotation with $1/D_r(L_i)$ (Eq. 1)	Rotation with $1/D_r(L_i)$ (Eq. 1)	l_e to L_i	Reptation, contour length fluctuation, constraint release

Note that the value of "p" in $\tau_R(L_i)/p^2$ sets the spectrum of Rouse motions, for unentangled micelles $p = 1,\cdots, N_{K,i}$; for entangled micelles $p = Z_i,\cdots, N_{K,i}$. Z and N_K are the number of entanglements and Kuhn

steps, respectively in the micelle. The subscript i represents micelles of length L_i. The detailed expressions for the above relaxation dynamics can be found either in Eq. 1 and 2 or our previous work.[32,33]

Reminiscent of our treatment of high frequency Rouse and bending motions, the dynamics of unentangled micelles are incorporated separately with an analytic form, rather than requiring simulations to obtain. Therefore these micelles are treated as relaxed (i.e., without any pointers on them) during the micelle breakage and reformation, in contrast to the entangled micelles for which loss of tube segments cause pointers to move along their backbone as the relaxation process continues. A flowchart with detailed information on the above simulation procedure can be found in the supplementary material, and the resulting linear rheological response of a partially entangled micelle solution can be expressed schematically by the mathematical formula given below:

$$G^*(\omega) = G^U(\omega, \langle L \rangle, l_e, l_p, d) + G^E(\omega, \varsigma, \langle L \rangle, l_e, l_p, d) \tag{3}$$

Here, G^* is the complex modulus, whose real and imaginary parts are G' and G" respectively. The superscripts U and E denote the contributions from unentangled and entangled micellar subpopulations, respectively. The relative breakage time is $\varsigma \equiv \bar{\tau}_{br}/\bar{\tau}_{rep}$, as defined by Cates,[29] whose magnitude manifests the effect of micellar breakage and re-formation on the reptation of entangled micelles (which is the slowest relaxation process with characteristic time $\bar{\tau}_{rep}$). The micelle diameter $d = 4\,nm$ used here was determined by SANS measurements. A similar expression for well-entangled WLMs can also be found in our previous work.[33]

Finally, it is noteworthy that in our simulations the micellar breakage/re-formation is modeled in a mean-field (MF) approach in that the breakage has the same rate per unit length regardless of

micelle length and location along the micelle. Thus, fusion of micelles is equally likely for micelles of any length and not correlated with previous breakage or fusion events, and no self-fusion is allowed, and hence there are no ring micelles. In addition, the entanglements are represented by a mean-field tube. These assumptions may not always hold. For example, breakage and fusion may occur in a single step, through a three-/four-arm branched intermediate structure that allows an end of one micelle to exchange with the end of another;[48] this would result in no creation of free ends, and thus lead to different rates of relaxation than is the case with uncorrelated breakage/re-formation. It is also possible that the fragments created by a breakage event might have a significantly higher probability of re-joining each other than of finding new partners with which to fuse, leading to correlations in breakage and fusion. There might also be non-uniform breakage, for example, preferably at the micelle end, as well as changes in length due to shedding/end evaporation of individual surfactant molecules.[46,49] These non-mean-field phenomena, as inferred from theories and simulations, can alter the concentration dependencies of micellar properties. The corresponding effects on the linear viscoelasticity would then not be captured by simply varying the value of ς. In particular, if the solution becomes diffusion controlled, and the fragments of a recently broken micelle are more likely to recombine with themselves than with other micelles, and kinetically-induced local perturbations from the equilibrium cannot be effectively averaged out. Under these circumstances, even though some assumptions made in the Cates theory might still hold, the properties of a micellar solution become non-mean-field and thus depend on specific mechanisms, especially for systems undergoing morphology change or phase transition.[46,48] However, as shown at the end of the paper, such non-mean-field effects remain of marginal significance as long as the micelles are entangled.

4. Results and Analysis

Since our aim is to understand the relationships between micelle microstructure and both slow and the fast dynamics for partially entangled WLM solutions through a combination of macro- and micro-rheology, the surfactant concentration of 1.5 wt. % was chosen not only because it is low enough that unentangled micelles are relatively prevalent, but it is also high enough that there is a significant rheological response over a frequency window that is accessible to both mechanical rheology and micro-rheological methods. In general, micro-rheology, including diffusing wave spectroscopy (DWS), as well as video and laser particle tracking techniques, can access much higher frequencies ($10 \sim 10^5$ rad/s) than can mechanical rheometry, with the upper limit of the former set by the Brownian motion of small probe particles. The rheological modulus is then calculated based on the use of the fluctuation-dissipation theorem, where the thermal motion of the probe particles is monitored and directly related to the viscoelasticity of the solution.[27,28,35] Thus, by combining high-frequency micro-rheological data with macro-rheological data at low frequencies ($0.1 \sim 300$ rad/s), a range of over six decades in frequency can be covered. This provides data that reflect dynamics over a wide range of micelle characteristic lengths, that can be assessed through our simulation model. However, precautions are needed when handling the above two sets of data, since discrepancies are usually observed between micro- and macro-rheological data possibly due to the inertia of the mechanical rheometer and due to probe-micelle interactions that affect the DWS measurements.[27,50] Therefore a data merging procedure is developed here to minimize artifacts associated with these disparities, with the details given in the supplementary material. Examples of the resulting combined rheological data for SLE1S+CAPB WLM solutions at different concentrations of salt, expressed as the total concentration of counterions [Na+], are given in Fig. 1.
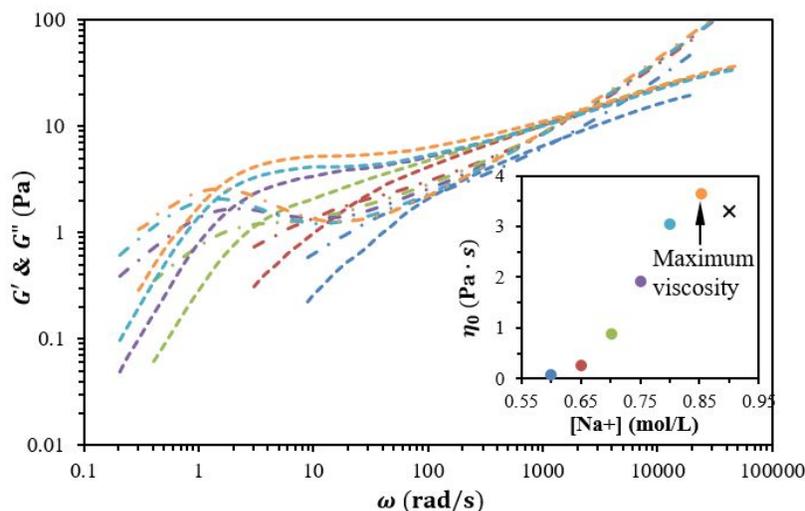
Figure 1. The combined rheological response (from mechanical rheometry at low frequencies and DWS at high frequencies) for WLM solutions (1.5 wt. % SLE1S+CAPB) with different sodium ion concentrations at 25 °C, where the line colors for different [Na⁺] concentrations are can be found in the inserted figure giving the corresponding zero shear viscosities. The maximum value of the zero shear viscosity is indicated in the inserted plot. The point beyond the maximum is denoted by an "X," as the corresponding G' and G" curves are omitted from the main graph. Dashed lines are G'; dot-dashed ones are G''. Note that the [Na⁺] concentrations include contributions from both the surfactant counterion and the added NaCl salt.

According to Fig. 1, by increasing the ionic strength from [Na+]=0.601 M to 0.852 M, the terminal regime, below the low-frequency cross-over ω_{1c}, over which G' and G" approach power laws of -2 and -1 respectively, shifts to 100-fold lower frequencies while the gap between G' and G" at intermediate frequencies becomes more prominent. These behaviors are accompanied by sigmoidal-shaped upswing of zero shear viscosity η_0 (see the insert in Fig. 1) indicating different

mechanisms for micellar growth at low and high salt concentrations. However, at high frequency, a second crossover between G' and G" can be found, whose frequency ω_{2c} is nearly independent of salt level. This high frequency crossover, signaling a change from an elastic response dominated by collective dynamics among entangled micelles to viscous-dominant short-range intramicellar bending motions,[51-53] is known to reflect the rigidity of WLMs and can only be measured by DWS. Since ω_{2c} is entirely obtained from DWS and is free from the ambiguities related to the data merging process, this specific frequency can be used to estimate the value of the persistence length l_p, as described in our previous studies.[33]

Quantitatively, the determination of the salt effect on micellar structures by experimentation alone is a challenge, since there is no independent control of each characteristic length or time when varying the salt concentration. The addition of salt should, in general, cause micelles to grow as a result of a higher energy penalty for forming end-caps, but it might also affect the breakage time $\bar{\tau}_{br}$. Therefore, it is difficult to determine whether an increase of viscosity is due to a larger micelle length $\langle L \rangle$ or to a slower breakage and reformation of the structure. The above complications are embodied in the nontrivial changes in the predicted G' and G" curves (See Fig. 2) when using the micellar parameters as inputs for the simulation approach using the pointer algorithm described previously. Since our interest here is to understand how the different micellar length and time scales affect the linear rheology of partially entangled WLM solutions, before directly attempting to predict the rheological data in Fig. 1, in what follows some reference rheological predictions are carried out with the investigated parameters either fixed at their standard values (See Table 2) or allowed to vary within a specific range exemplifying the partially entangled regime.

Table 2. Standard values of micellar parameters used for simulation predictions in Fig. 2

Micellar parameters					Solution conditions		
ς	$\bar{Z}$	l_e(nm)	l_p(nm)	d (nm)	T (K)	ϕ	η_s (mPa.s)
100	3	300	50	4	300	0.01	0.85
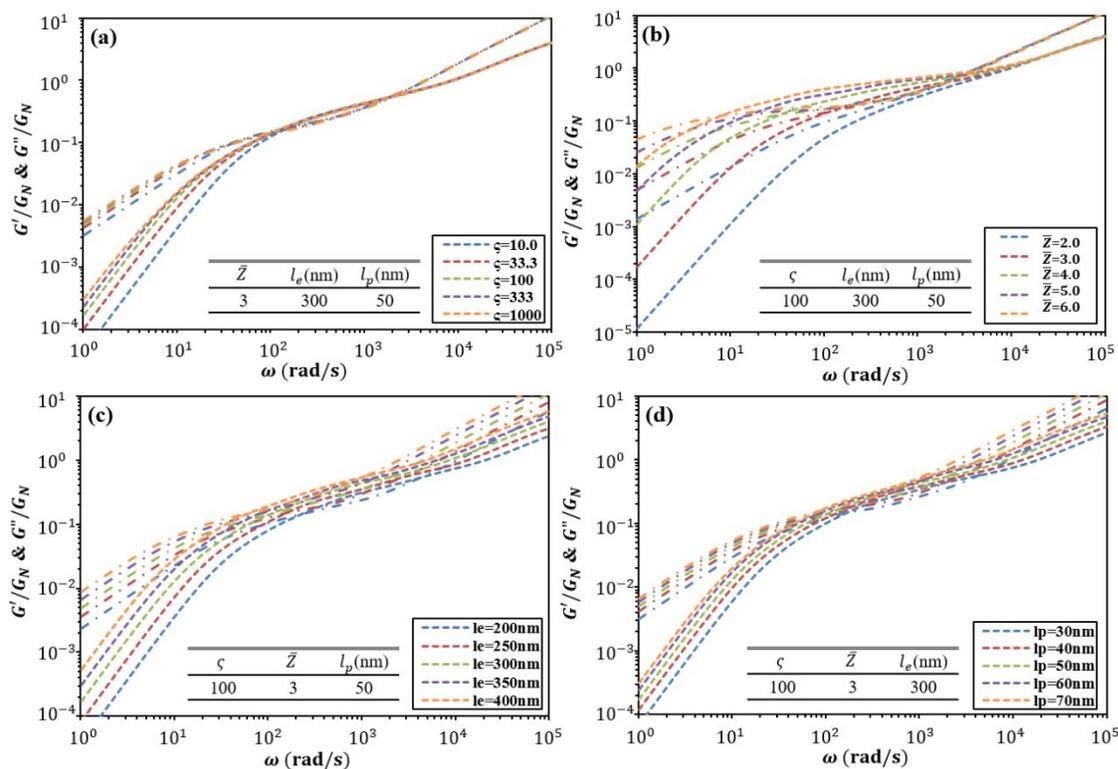
Figure 2. Effect of each of the following micellar parameters on normalized G'/G$_N$ (dashed lines) and G''/G$_N$ (dot-dashed lines): (a) ς, (b) $\bar{Z}$, (c) l_e, (d) l_p. The inserted tables indicate the parameters that are fixed at their standard values.

As shown by Fig. 2a, ς, the dimensionless micelle breakage and reformation time, has its greatest influence at low frequencies: a larger ς shifts the terminal regime to lower frequencies, as WLMs

relax more slowly because of less frequent breakage/re-formation. $\bar{Z}$ governs the transition between entangled and unentangled systems; at small $\bar{Z}$, micelles are barely entangled, and the predicted rheological response is similar to that for dilute solutions of rigid or semiflexible rods,[54-56] for which the loss modulus (G") exceeds the storage modulus (G') over the entire frequency spectrum. However, by increasing $\bar{Z}$ (with l_e and l_p fixed), the terminal behavior is extended to ever lower frequencies, giving rise to a broader frequency window over which the elastic response (G') is dominant, showing clearly the emergence of a transient network of entangled WLMs. In principle, the width of this elastic-dominant frequency window $w_E=\omega_{2c}/\omega_{1c}$ (i.e., the ratio of high frequency to low frequency crossovers), should be rather sensitive to $\bar{Z}$ whose value determines the density of the transient network formed by entanglements. Thus, by plotting w_E vs $\bar{Z}$ for $\bar{Z}$ between 2.5 and 6.0 (See Fig. 3), we obtained the following power law correlation:

$$w_E \cong C(l_e,l_p)(\bar{Z}-\bar{Z}_c)^{2.4} \text{ for } \bar{Z} > \bar{Z}_c \qquad (4)$$

Here, $\bar{Z}_c = 2$ is the critical entanglement number, which sets the threshold for the formation of the entangled network, heralded by the rise of G' above G" at a critical frequency, which immediate splits into two crossovers of the G' and G" curves (see Fig. 2b). $C(l_e,l_p) \approx 19.5$ is a prefactor weakly dependent on micelle local length scales l_e and l_p for $\varsigma > 1$, for which the breakage and re-formation are too slow to effect w_E as shown by Fig. 2a.
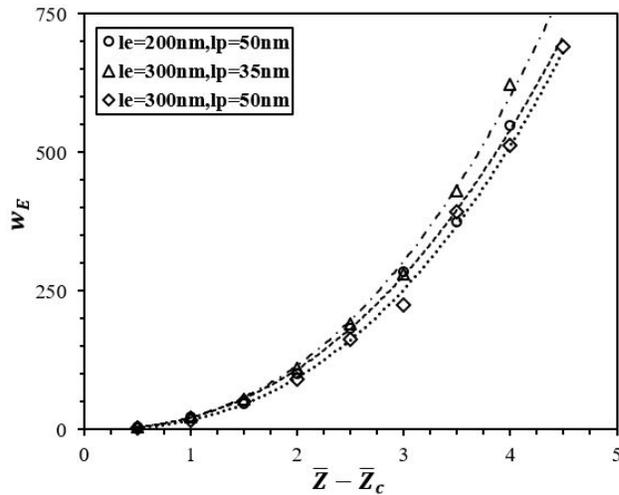
Figure 3. Empirical correlation for the dependence of $w_E = \omega_{2c}/\omega_{1c}$ on $\overline{Z}$ at various l_e and l_p with standard value of $\varsigma = 100$ (given in Table 2). R^2 values are all larger than 0.997 for the following three fits in the figure, i.e., $w_E = 22.41(\overline{Z} - 2)^{2.37}$ for the dash-dotted line, $w_E = 21.91(\overline{Z} - 2)^{2.31}$ for the dashed line, and $w_E = 17.08(\overline{Z} - 2)^{2.45}$ for the dotted line.

To understand the further changes of G' and G" curves shown in Fig. 2c and d, one would need to think of a micelle as a thread of correlation 'blobs',[57] whose size is governed by both the entanglement length (l_e) and the rigidity of the WLMs (l_p). For micelles containing a fixed number of entanglements $\overline{Z}$, the consequences of a larger correlation length (i.e., a larger l_e or l_p see Fig. 2c and d) are two-fold: an increase in the tube length along which micelles must diffuse, thereby increasing the terminal relaxation time on one hand and a shifting of high frequency dynamics including Rouse and bending motions (manifested by a scaling law of 0.5 and 0.75 at high frequencies) to later times or lower frequencies on the other. A combination of these two effects eventually leads to leftward shifts in both the low- and the high-frequency linear rheology.

As a well-established method for characterizing molecular assemblies in an isotropic medium, SANS has long been used to determine the size and the shape of micelles from the scattering spectra.[58-60] Since WLMs usually have a hydrophobic core dense in hydrogen atoms, which facilitate scattering from the surfactant-water interface, a worm-like micelle can be modeled as a freely jointed chain of subunits carrying form factors of rigid cylinders, each of length (L_1) equal to the Kuhn length, which is twice the persistence length. By fitting experimental scattering intensity $I(q)$ with a recently developed hybrid function at both high- and low-q regions,[36] the diameter ($d = 2R_1$) and persistence length ($l_p = L_1/2$) as well as the overall micelle length $\langle L \rangle$ can be thereby measured for dilute WLM solutions.[37] However, at higher concentrations, when micelles are long enough to overlap and form entanglements, quantitative estimation of $\langle L \rangle$ becomes impossible because the magnitude of the scattering within the lower q range is set by the screening length rather than by $\langle L \rangle$. Such a limitation in scattering, we believe, can be partly resolved by investigating the rheology of nearly dilute WLM solutions through the simulation model described previously, so that some of the larger-scale characteristic lengths can be inferred from rheological measurements, thus supplementing the small-scale lengths inferred from scattering. Thus, to compare characterization data inferred from rheology with that inferred from SANS, we chose appropriate concentrations to allow independent analyses of the data from both rheometry (See Fig. 1) and scattering as a function of salt concentration. For SANS, the maximum concentration for extracting micelle length is usually between 0.1 and 0.5 wt. %, which is lower than the minimum needed for rheology (1.0~2.0 wt. %), which leaves an "inaccessible" zone of concentrations between these limits over which neither SANS nor rheology is able to yield a reliable estimate of $\langle L \rangle$. Figure 4 shows the scattering intensities of 0.20 wt. % WLM solutions at three different salt concentrations, where the small changes in $I(q)$ at the intermediate and high q

regions indicate that salt has only subtle effects on the micelle diameter d and persistence length l_p for the given range of added salts. However, the steady rise of low-q intensity upon addition of salt signifies the growth of micelle length in agreement with results from linear rheology (Fig. 1) as discussed earlier in this section.
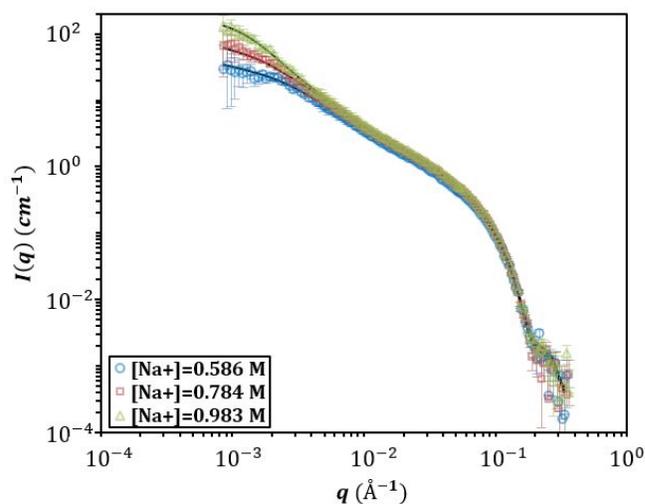
Figure 4. SANS scattering intensity $I(q)$ for 0.20 wt. % of WLM solutions at 25 °C with different [Na+] which includes contributions from both the counterion for the surfactant and from the added salt. Note that the fits (solid lines) in the figure are achieved through a hybrid scattering function in reference.[36]

5. Discussion

Although one could predict the linear rheological response from a given set of micellar parameters as demonstrated by Fig. 2, to solve the corresponding inverse problem, i.e., to estimate micellar parameters on the basis of experimentally determined G' and G" curves, calls for a sophisticated optimization procedure, where micellar parameters are adjusted iteratively to

minimize the deviations between experiment and simulation results. Each micelle parameter has its greatest effect on specific ranges of the G' and G" curves.[32] To take advantage of this, we divide the accessible frequency window into multiple regions bounded by local features, for instance, the crossovers at low and high frequencies. Averaged deviations between experimental measurements and simulation predictions as well as the differences in local features are then calculated so that micellar parameters can be tuned accordingly through a set of empirical correlations, for example Eq. 4, which link a local change of G' and G" curves to a corresponding modification of micellar parameters. Some of these empirical formulas are borrowed from our previous work for well-entangled WLMs,[32,33] and a detailed description of the parameter optimization can be found in the supplementary material. Through this procedure, we extract the micellar parameters from the rheological data shown in Fig. 1 for different concentrations of salt, and the resulting simulated vs measured G' and G" curves corresponding to the lowest ([Na+] = 0.601 M) and the highest ([Na+] = 0.852 M) salt concentration are given in Fig. 5. Results for solutions at other salt concentrations are shown in Fig. S5 in the supplementary material.
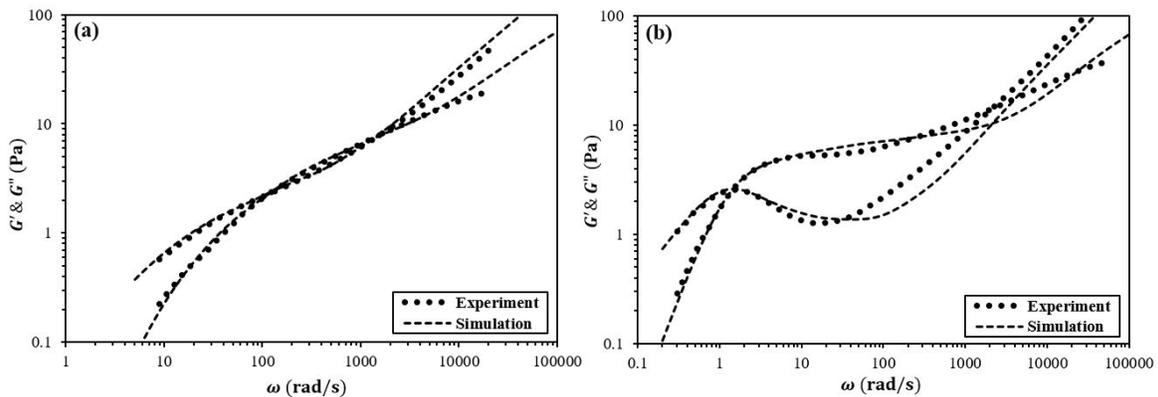
Figure 5. Data (symbols) for linear rheological measurements compared with the corresponding fits (lines) from simulations for both (a) partially entangled and (b) well-entangled micelle solutions at 25 °C at the same surfactant weight fraction (1.5 wt. % SLE1S+CAPB) but at concentrations of [Na+] of (a) 0.601 M and (b) 0.852 M, which include ions from both surfactants and added salt.

In Fig. 5a, where micelles are partially entangled, less than 6% absolute average fitting deviations are obtained between experimental and simulated rheology over three decades of oscillation frequency, which clearly demonstrates that our simulation model can nearly quantitatively capture the rheological behavior of partially entangled WLM solutions. However, as illustrated in Fig. 5b, there exist mismatches between predicted and measured rheological responses in the limit of high frequencies, which, we believe, are due to the limitations of the experimental techniques, i.e., the inaccurate estimation of elastic modulus from DWS. It is generally accepted this is mainly due to slip and the compression of fluid at the interface between probe particle and viscoelastic medium as well as possible particle-micelle interactions.[27,48] As elaborated in the supplementary material, the high frequency DWS data is merged with those from mechanical rheometry through a vertical shift of the former which is routinely used to allow for the best data overlap at intermediate frequencies (50-150 rad/s). Thus, only the high frequency crossover ω_{2c} is used from DWS to extract the micellar persistence length. Hence, neither the amount of vertical shift of DWS data, nor any other deviations between theory and experiments at high frequencies, other than the cross-over frequency, have any effect on the determination of l_p.

Table 3. Summary of "insensitivity percentages" (defined in the text) for micellar parameters of partially entangled WLM solutions (1.5 wt. % SLE1S+CAPB with [Na+]=0.601 M) at 25 °C. For the partially entangled solutions, two columns are given. In the first column for "Freely fitted l_p," all parameters (including l_p), are adjusted freely to obtain a best fit, except that the parameter in the row heading is set to a series of fixed values that deviate from its best-fit value, to determine how large this deviation can be without forcing significant error (> 10%) in the overall average fit. For the column labeled "Fixed l_p (=32 nm)," the procedure is the same, except that l_p is held fixed at 32 nm while other parameters (except the parameter in the row heading) are adjusted to give a best fit.

	Insensitivity percentages		
Parameter	Partially entangled solution		Well-entangled solution
	Freely fitted l_p	Fixed l_p (=32 nm)	
$\bar{Z}$	±8%	±6%	±20%
l_e	> 240 nm*	±7.5%	±7.5%
l_p	< 45 nm*	~	±15%
ς	> 40*	> 40*	±25%
G_N	±15%	±12.5%	±10%
$\langle L \rangle$	±15%	±12.5%	±30%

Note that for partially entangled solutions, the linear rheology is insensitive to some micelle parameters when those parameters are in the range given by the inequalities, marked by * in the table. The insensitivity percentages for well-entangled micelle solution are from our previous work.[33]

The salt concentration-dependent micellar properties obtained by fitting the rheological data with the model are shown in Fig. 6, with the accuracies of estimates assessed using the results of sensitivity studies given in Table 3. The sensitivity studies are carried out by performing a constrained fit in which one parameter at a time is fixed at a value that deviates from the best-fit

one by a given percentage. The goodness of the fit after optimizing values of other parameters gives a measure of the sensitivity of the constrained parameter to error or noise. We then define the "insensitivity percentage," to be the percentage variation that the constrained parameter can be allowed to vary from the best-fit value, changing other parameters to compensate to the extent possible, while keeping the average absolute fitting error to be less than 10 %. Since the same analysis has been elaborated for well-entangled WLMs in our previous work,[33] only insensitivity percentages for the partially entangled system ([Na+] = 0.601 M) are determined here; the results for well-entangled WLMs presented in Table 3 are taken from previous work.

Table 3 shows a much smaller insensitivity percentage for $\bar{Z}$ for partially entangled micelles than for well-entangled WLM solutions,[33] implying a higher accuracy in estimating entanglement number when solutions are partially entangled. This is consistent with the observations from Fig. 2b for partially entangled micelles: a moderate change in $\bar{Z}$ leads to a dramatic alteration in predicted rheological response, which is not surprising since with only a small increase in $\bar{Z}$ a number of micelles are converted from unentangled to entangled, which significantly broadens the elastic-dominant frequency window (See Fig. 3). However, this decrease in uncertainty in $\bar{Z}$ in the partially entangled regime is not found for the other parameters. For example, l_e and l_p cannot be determined individually in the partially entangled regime because the effect on the G' and G" curves of varying one of them can be readily compensated by the adjustment of the other as long as $l_e > 240$ nm or $l_p < 45$ nm. (As shown in Fig. 2c and d, a shift of G' and G" curves to lower frequency by increasing l_e can be off-set by using a smaller value of l_p.) (For details, see Fig. S6b and c, Table S2 and 3 in the supplementary material.) This loss of sensitivity occurs because when solutions are dilute, the tube becomes fat so that the difference in characteristic times between the

reptation of the chain and the Rouse motion within the tube segments becomes relatively small, which makes accurate estimations of l_e and l_p difficult as these two length scales are correlated with each other through the plateau modulus. Since neutron scattering techniques are especially suitable to characterize structures with length scales of hundreds of nanometers or less, SANS could be used to determine l_p and then this value could be used when estimating other micellar parameters through our simulation model. According to the column labeled "Fixed l_p" in Table 3, this results in a much higher accuracy (7.5%) in estimating l_e from rheology, and it also helps to improve the estimates of other parameters, bringing their sensitivities close to, or even better than, those of well-entangled WLM solutions, except for ς. As illustrated by Fig. 2b, for ς >> 1, the value of ς has only a minimal effect on the terminal region of G' and G" curves, making it impossible to ascertain the value of ς from rheology, especially when the solution is less viscous. The reason for this insensitivity is that for ς >> 1 the micelles rarely break before relaxing by reptation, and so the breakage rate no longer affects the rheology.
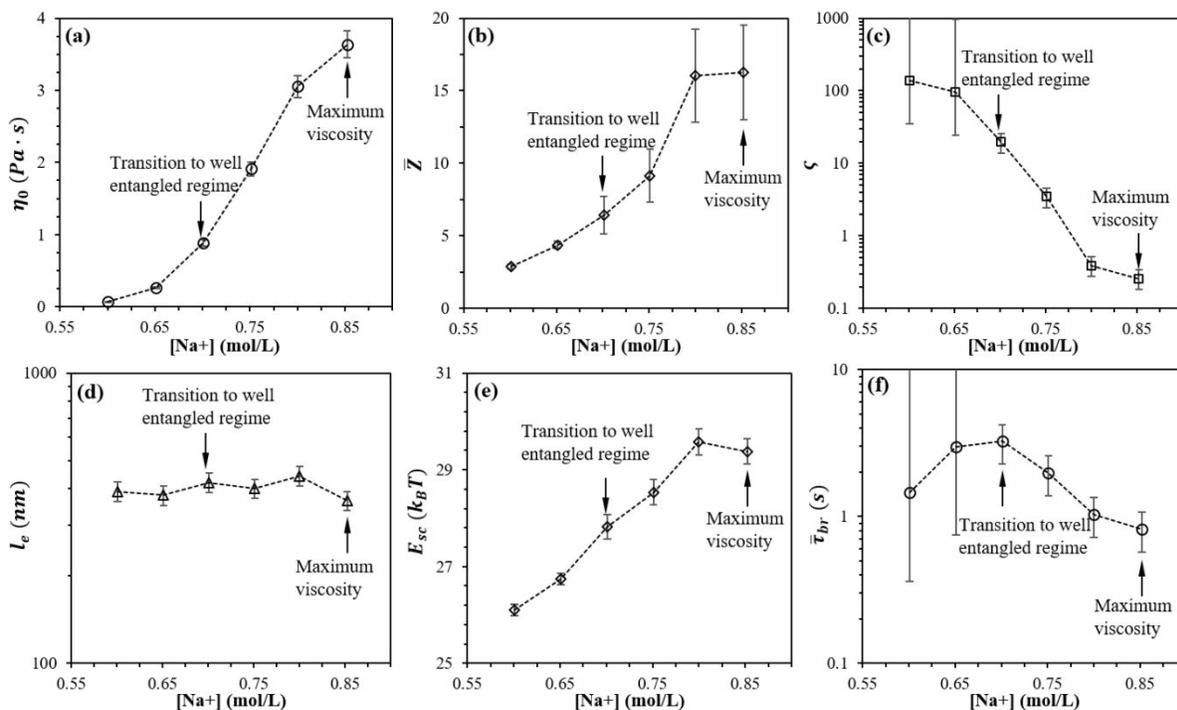
Figure 6. The dependence of characteristic micellar properties on salt concentration. (a) η_0 determined experimentally. The remaining sub-figures are the parameters obtained from fitting the rheometric measurements shown in Fig. 1, namely: (b) the average entanglement number $\bar{Z}$; (c) the ratio of breakage time to reptation time ς; (d) the entanglement length l_e; (e) the scission free energy E_{sc}; (f) the average breakage time $\bar{\tau}_{br}$. The error bars are generated using their insensitivity percentages in Table 3. The transition to the well-entangled regime (i.e., when only 10% micelles on average are unentangled, which is the case for [Na+] = 0.701 M) and positions of the zero shear viscosity maxima are indicated in the above figures.

Added salts produce screening of electrostatic repulsion among surfactant molecules, allowing head groups to pack more tightly, leading to a higher free energy penalty for forming micellar end-caps. This produces a steep increase in solution viscosity η_0, number of entanglements $\bar{Z}$, as well

as a decrease in the ratio of breakage to reptation time ς, as shown in Fig. 6a, b, and c, respectively: $\bar{Z}$ doubles while ς drops 100-fold along with a nearly exponential rise in η_0 as [Na+] increases only from 0.601 to 0.701 M. This clearly indicates a transition from a partially entangled to a well entangled solution. (According to our model, 30% of the micelles are unentangled at [Na+] = 0.601 M, and only 10% remain unentangled at [Na+] = 0.701 M) Once sufficient salts are added to solutions, the screening length for electrostatic interactions between entangled WLMs should become small enough that the entanglement length l_e becomes a function of surfactant concentration only, which is confirmed in Fig. 6d, wherein a nearly constant l_e is obtained at different salt concentrations. However, with still more salt, the entanglement-triggered upswing of η_0 slows down as the micelle solution falls into the fast breakage regime ($\varsigma \leq 1$), where the relaxation is sped up by the micelle breakage and re-formation. According to Fig. 6e and f, this behavior corresponds to the competition between the elongation of WLMs owing to the increase of scission free energy E_{sc} and the acceleration of intermicellar breakage and reformation as illustrated by the reduction of $\bar{\tau}_{br}$ shown in Fig. 6f. The scission free energy E_{sc} is the penalty for forming two micellar end-caps by breakage of a WLM, which is calculated from the predicted micelle length through Eq. 5, presented below. The appearance of micellar branches may also contribute to the slow down in growth of η_0 with added salt.

Because of the incomplete screening at low salt concentration, the persistence length is thought to be large at low salt, gradually decreasing to a constant as the micelle charge is screened by added salt, eventually making the micelle effectively neutral. Perhaps because of the uncertainty in estimation of l_p from rheology as well as the very limited range of salt concentrations studied here,

we do not observe such a decrease in micelle persistence length. According to Fig. 7a, a nearly constant l_p is determined from both rheology and SANS with varying salt concentration, which implies that charges on the micelles are largely already screened out even before the onset of entanglements. As confirmed by Fig. 7a, even though SANS measurements are obtained from WLM solutions with a lower concentration (7.5 times lower) than those for rheology, the estimations of l_p from these two methods are relatively close: from SANS, $l_p \cong 30\ nm$ and from rheology $l_p \cong 40\ nm$. In contrast to l_p and other local length scales (i.e., d and l_e) of WLMs, the average length of the micelle $\langle L \rangle$ depends on both the concentration of the solution and the scission free energy E_{sc} as described by the following expression, derived from ideal mixing of micelles and single surfactant molecules in equilibrium:[44]

$$\langle L \rangle \cong \frac{8\overline{M}_s \chi^{0.5}}{\rho_s \pi d^2 N_A} \exp\left(\frac{E_{sc}}{2k_B T}\right) \tag{5}$$

where χ is the mole fraction of surfactants, $\overline{M}_s = 346.66$ g/mol and $\rho_s = 1.12$ g/cm^3 are the average molecular weight and density of the surfactants, respectively. N_A is Avogadro's number. From Eq. 5, if we assume E_{sc} is a function of salt concentration only, at the same concentration of added salt, the predicted $\langle L \rangle$ from rheology and SANS should be different by the square root of the concentration ratio of the surfactant, i.e., $\sqrt{7.5}$ which is fairly consistent with Fig. 7b at low salt concentrations. However, at high salt concentration, where micelle breakage and re-formation become more important, rheology gives a higher value of $\langle L \rangle$ than we would infer by re-scaling the value from SANS by $\sqrt{7.5}$. A possible explanation is that the square root scaling law

dependence of $\langle L \rangle$ on surfactant concentration, derived from mean-field theory, does not hold over the transition between unentangled and entangled solutions.
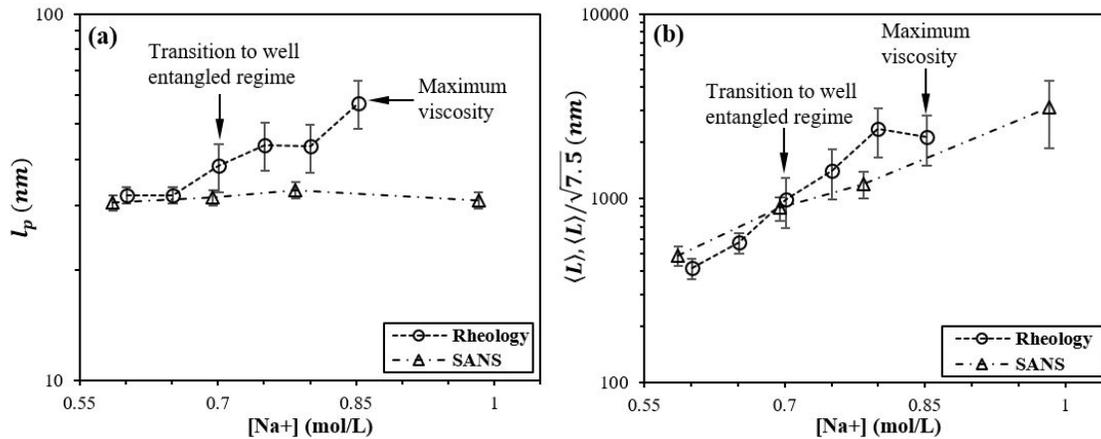
Figure 7. Comparisons of the estimated (a) l_p and (b) $\langle L \rangle$ from rheology and SANS for WLM solutions at various salt concentrations. Note that to compensate the difference in surfactant concentration between SANS (0.2 wt. %) and rheological measurements (1.5 wt. %), values of $\langle L \rangle$ determined from rheology are reduced by a factor of the square root of the concentration ratio, $\sqrt{7.5}$. Error bars of the parameters estimated from rheology are based on their insensitivity percentages (See Table 3).

One might argue that the mean-field (MF) picture might fail as the solution concentration drops into the partially entangled regime; in that event a single parameter, i.e., ς or $\bar{\tau}_{br}$, would fail to describe the micelle breakage and re-formation. Since the rate at which one micelle can diffuse towards another to allow the two to fuse depends on the average distance between micelles, a possible transition from mean-field (MF) reaction-controlled (RC) to diffusion-controlled (DC) fusion may affect the rheological properties.[61] Under diffusion-controlled fusion, a newly-created

micelle end is more likely to recombine with its original partner from the preceding breakage than with its surrounding neighbors. This phenomenon is called "self-recombination" in which the initial chain length can only be forgotten after multiple breakage and re-formation events. In this case, a long WLM would become contaminated with short relaxed regions, as fresh micelle ends created by breakage relax slightly by fluctuation, and then rejoin by self-recombination. It has been suggested that this non-mean-field diffusion-controlled (DC) fusion of micelles might be responsible for the anomalous short-time and fat-tailed late-time relaxations observed in some micelle solutions.[62,63]

Since at present, there is no rigorous theory available for reaction kinetics in WLM solutions where $\bar{\tau}_{br}$ changes with both surfactant and salt concentrations,[31,46,64] we here use scaling arguments from O'Shaughnessy and Yu[63] to assess the importance of non-MF effects. DC kinetics result from slower reaction between adjacent micelles than that set by diffusion, and according to O'Shaughnessy and Yu,[63] this occurs when the $\varsigma_{DC} \equiv \bar{\tau}_D/\bar{\tau}_{rec} \gg 1$. Here $\bar{\tau}_D$ and $\bar{\tau}_{rec}$ are the average diffusion time and the average recombination time for a micelle end to reach and fuse with its nearest neighbors, respectively. If the solution is in the entangled regime, the diffusion distance is controlled either by reptation ($\sim t^{1/4}$) at early times when the micelle is confined to its tube, and by center of mass diffusion ($\sim t^{1/2}$) at later times when the micelle has escaped its tube. If the micelles are unentangled, this distance is controlled by translational diffusion ($\sim t^{1/2}$) for unentangled micelle rods. These three situations give the following formulas for ς_{DC}:

$$\varsigma_{DC} \equiv \frac{\bar{\tau}_D}{\bar{\tau}_{rec}} = \begin{cases} \left(\dfrac{\bar{\tau}_D}{\bar{\tau}_{br}}\right)^4 & \text{for entangled solutions at early times} \\[2em] \left(\dfrac{\bar{\tau}_{br}^{2/3}\bar{\tau}_{rep}^{1/2}}{\bar{\tau}_D^{1/6}\bar{\tau}_G}\right)^3 & \text{for entangled solutions at late times} \\[2em] \left(\dfrac{\bar{\tau}_{br}}{\bar{\tau}_D}\right)^2 & \text{for unentangled solutions at all times} \end{cases} \quad (6)$$

Here, $\bar{\tau}_{rep}$ and $\bar{\tau}_G$ are the characteristic times for reptation and center of mass diffusion, respectively. Through detailed analyses deriving and analyzing the above expressions in the supplementary material, we find that with ϕ=1.51% (SLE1S+CAPB) the well entangled micelle solution ([Na+]=0.852 M) is deeply within the reaction-controlled, mean-field regime, and the partially entangled solution ([Na+]=0.601 M) is in a marginal state where the mean-field theory is starting to break down. Dilute micelle solutions (i.e., ϕ=0.20 % with characteristic length scales inferred from SANS) are well within the diffusion-controlled regime, where the mean-field theory fails. This conclusion emerges, because when a micelle in dilute solution breaks, the two pieces are more likely to both find each other and react before another, more distant micelle, can do so. Well entangled micelles have many nearby micelles that can react with a fragment of a micelle before it finds and reacts with the fragment from which it broke free. However, since the SANS results provide only equilibrium properties, and no dynamics, this breakdown of mean-field theory has no impact on the SANS results or their interpretation.

By assuming $\langle L\rangle \sim \phi^\nu$, (with ν=1/2 for MF entangled WLM solutions,[29] and ν usually larger than 1/2, taken here to be 3/5, for dilute surfactant solutions.[49,66]) we obtain the following scaling laws for ς_{DC} vs ϕ: (See supplementary material for detailed derivations)

$$\varsigma_{DC} \sim \phi^{\alpha} \quad \alpha = \begin{cases} 4(3\nu - 1) = 2 & \text{for entangled solutions at short times} \\ -4\nu = -2 & \text{for entangled solutions at long times} \\ 4 & \\ \frac{4}{3}(1 - 4\nu) = -\frac{28}{15} & \text{for unentangled solutions at all times} \end{cases} \quad (7)$$

Thus, on the basis of the above estimates of ς_{DC}, and the concentration scaling law given above, the MF picture for the surfactant solutions studied here should be valid over the range of concentrations over which the micelles remain threadlike and well entangled without dense branching. While one expects the exponent ν to be 1/2 in the well-entangled regime due to coil overlap, and thus the mean-field to become better at higher concentrations, if branches proliferate, and a network of intramicellar loops form, self-reaction of micelles may become common, leading to a high-concentration deviation from mean-field theory. The existence of micellar loops could greatly retard the overall relaxation of the micelle solution, which is a possible explanation for the observed low frequency plateau in G' as reported in the literature.[67]

The above arguments suggest that mean-field scission and recombination likely govern much of the interesting regime of WLM rheology outside of the highly branched regime. Thus, for unbranched micelles, the linear viscoelastic regime is now quite well understood. Future work can thus focus on understanding how the nonlinear flow behavior can benefit from the knowledge of microstructure inferred by the characterization in linear regime. In fact, up to now, only qualitative or incomplete explanations of the nonlinear rheology of WLM solutions have been proposed.[68,69] The flow-induced orientation of micelles, as well as their flow-induced migration, banding, as well as the disintegration of large micellar clusters are presumably representative of the interplay

between time scales set by the flow and those set by micellar diffusion, breakage, and re-formation.[11,70,71] By providing quantitative information on micellar properties, our work, we believe, should shed insight on the evolution of micellar structure under large deformations, and therefore lay a solid framework for the establishment of nonlinear rheological models for WLM solutions in the future. Future work should also focus on including the effects of micelle branching on the linear viscoelastic properties, and eventually the nonlinear properties, of worm-like micelle solutions.

6. Conclusion

We have carried out a quantitative investigation of mesoscale structures of partially entangled WLM solutions with the characteristic lengths and times extracted through a combination of mesoscopic simulation at the level of micellar dynamics and experimental techniques including both macro- and micro-rheology, namely diffusing wave spectroscopy (DWS) as well as neutron scattering. By including additional relaxation mechanisms for unentangled micelles, our recently developed pointer algorithm for entangled WLMs solutions has been extended to enable characterization of solutions that are partially entangled with a much lower viscosity. With high-frequency data obtained from DWS, the extended model is able to predict the linear rheological response (G' and G'' curves) for partially entangled WLM solutions with less than 7% absolute average deviation from experimental mechanical rheometry measurements through our established data merging and fitting procedures. The accuracies of the predicted micellar parameters was assessed by sensitivity studies, which show larger uncertainties in determination of micelle entanglement length and persistence length as well as breakage time than for well-entangled solutions. Both the number of entanglements and the breakage time obtained from this model

showed steep changes as functions of salt concentration, while the entanglement length remained nearly constant across the transition between unentangled and entangled micelles. The estimated persistence length l_p and micelle length from rheological measurements were consistent with those from SANS results for WLM solutions with the same total concentration of counterions [Na+]: for SANS $l_p \cong 30\, nm$ and for rheology $l_p \cong 40\, nm$. Allowing for the difference in surfactant concentration between the rheological and SANS experiments, the micelle lengths extracted from rheology are consistent with those from SANS except at high [Na+] where micelle breakage and reformation becomes important and rheology gives a roughly two-fold higher value of $\langle L \rangle$ than does SANS. This is, to our knowledge, the first time that quantitative comparisons of structural features including micelle length are made between rheology and SANS. Scaling arguments lead to the conclusion that the WLM solution breakage and fusion rates are reaction-controlled, and therefore described by mean-field theory over the entire range of concentration of entangled thread-like micelles, although with sufficient dilution, a diffusion-controlled regime should eventually be achieved. Mean-field theory may also fail at high surfactant concentrations, and high levels of branching, where intramicelle loops may form within branched micelle clusters, giving rise to an elastic plateau regime at low frequencies.

Acknowledgements

Supporting information

Flow chart of simulation procedure, method for combining macro- and micro-rheological experimental data, derivation of the ratio of micelle diffusion time to recombination time for the entangled and unentangled regimes

References

(1) Crothers, M.; Zhou, Z. Y.; Ricardo, N. M. P. S.; Yang, Z.; Taboada, P., Chaibun-dit, C.; Attwood, D.; Booth, C. Solubilisation in Aqueous Micellar Solutions of Block Copoly(oxyalkylene)s. *Int. J. Pharm.* **2005**, *293*, 91–100.

(2) Kunieda, H.; Horii, M.; Koyama, M.; Sakamoto, K. Solubilization of Polar Oils in Surfactant Self-organized Structures. *J. Colloid Interface Sci.* **2001**, *236*, 78–84.

(3) Huang, J.; Zhang, S.; Feng, Y.; Li, J.; Yan, H.; He, F.; Wang, G.; Liu, Y.; Wang, L. Rheological Properties and Application of Wormlike Micelles Formed by Sodium Oleate/benzyltrimethyl Ammonium Bromide. *Colloids and Surfaces A: Physicochem. Eng. Aspects* **2016**, *500*, 222–229.

(4) Gao, S.; Sun, T.; Chen, Q.; and Shen, X. Characterization of Reversed Micelles Formed in Solvent Extraction of Thorium(IV) by Bis(2-ethylhexyl) Phosphoric Acid. Transforming from Rodlike to Wormlike Morphology. *Radiochim. Acta* **2016**, *104*, 457–469.

(5) Lin, Z. Q.; Zheng, J. L. Y.; Davis, H. T.; Scriven, L. E.; Talmon, Y. Comparison of the Effects of Dimethyl and Dichloro Benzoate Counterions on Drag Reduction, Rheological Behaviour, and Microstructures of a Cationic Surfactant. *J. Rheol.* **2001**, *45*, 963–981.

(6) Kaler, E. W.; Murthy, A. K.; Rodriguez, B. E.; Zasadzinski, J. A. N. Spontaneous Vesicle Formation in Aqueous Mixtures of Single-Tailed Surfactants. *Science* **1989**, *245*, 1371-1374.

(7) Villeneuve, M.; Kaneshina, S.; Imae T.; and Aratono, M. Vesicle-Micelle Equilibrium of Anionic and Cationic Surfactant Mixture Studied by Surface Tension. *Langmuir* **1999**, *15*, 2029–2036.

(8) Wang, A.; Shi, W.; Huang, J.; and Yan, Y. Adaptive Soft Molecular Self-assemblies. *Soft Matter* **2016**, *12*, 337–357.

(9) Adamy, S. T. Viscoelastic Behavior of Alkyl Ether Sulfate Systems Containing Sodium Carbonate. *J. Surfact. Deterg.* **2016**, *19*, 599–608.

(10) Oelschlaeger, C.; Willenbacher, N. Mixed Wormlike Micelles of Cationic Surfactants: Effect of the Cosurfactant Chain Length on the Bending Elasticity and Rheological Properties. *Colloids and Surfaces A: Physicochem. Eng. Aspects* **2012**, *406*, 31– 37.

(11) Zhao, Y.; Haward, S. J.; Shen, A. Q. Rheological Characterizations of Wormlike Micellar Solutions Containing Cationic Surfactant and Anionic Hydrotropic Salt. *J. Rheol*. **2015**, *59*, 1229-1259.

(12) Lonetti, B.; Tsigkri, A.; Lang, P. R.; Stellbrink, J.; Willner, L.; Kohlbrecher, J.; and Lettinga, M. P. Full Characterization of PB-PEO Wormlike Micelles at Varying Solvent Selectivity. *Macromolecules* **2011**, *44*, 3583–3593.

(13) Dai, C.; Li, W.; Cui, Y.; Sun, Y.; Wu, W.; Xu, Z.; Liu, Y.; Yanga, Z.; Wu, X. The Effect of Functional Groups on the Sphere-to-wormlike Micellar Transition in Quaternary Ammonium Surfactant Solutions. *Colloids and Surfaces A: Physicochem. Eng. Aspects* **2016**, *500*, 32–39.

(14) da Silva, G. C.; Rossi, C. G. F. T.; Dantas Neto, A. A.; Dantas, T. N. C.; Fonseca, J. L. C. Characterization of Wormlike Micellar Systems Using DLS, Rheometry and Tensiometry. *Colloids and Surfaces A: Physicochem. Eng. Aspects* **2011**, *377*, 35–43.

(15) Padalkar, K. V.; Gaikar, V. G.; Aswal V. K. Characterization of Mixed Micelles of Sodium Cumene Sulfonate with Sodium Dodecyl Sulfate and Cetyl Trimethylammonium Bromide by SANS, FTIR Spectroscopy and NMR Spectroscopy. *J. Mol. Liq.* **2009**, *114*, 40-49.

(16) Padalkar, K. V.; Pal, O. R.; Gaikar, V. G. Rheological Characterization of Mixtures of Cetyl Trimethylammonium Bromide and Sodium Butyl Benzene Sulfonate in Aqueous Solutions. *J. Mol. Liq.* **2012**, *173*, 18-28.

(17) Hideki, S.; Yoichi, O.; Hideki, K.; Atsutoshi, M.; Takahiro, O.; Koji, T.; Masahiko, A. Photoinduced Reversible Change of Fluid Viscosity. *J. Am. Chem. Soc.* **2005**, *127*, 13454–13455.

(18) Lu, H.; Yang, L.; Wang, B.; and Huang, Z. Switchable Spherical-wormlike Micelle Transition in Sodium Oleate/N-(3-(dimethylamino)propyl)-octanamide Aqueous System Induced by Carbon Dioxide Stimuli and pH Regulation. *J. Disper. Sci. Technol.* **2016**, *37*, 159-165.

(19) Lu, H.; Shi, Q.; Wang, B.; Huang, Z. Spherical-to-wormlike Micelle Transition in a Pseudogemini Surfactant System with Two Types of Effective pH-responsive Groups. *Colloids and Surfaces A: Physicochem. Eng. Aspects* **2016**, *494*, 74–80.

(20) Clausen, T. M.; Vinson, P. K.; Minter, J. R.; Davis, H. T.; Talmon, Y.; Miller, W. G. Viscoelastic Micellar Solutions: Microscopy and Rheology. *J. Phys. Chem.* **1992**, *96*, 474-484.

(21) Lin, Z. Branched Worm-like Micelles and Their Networks. *Langmuir* **1996**, *12*, 1729-1737.

(22) Yusof, N. S. M.; Khan, M. N.; and Ashokkumar, M. Characterization of the Structural Transitions in CTAB Micelles Using Fluorescein Isothiocyanate. *J. Phys. Chem. C* **2012**, *116*, 15019−15027.

(23) Kalur, G. C.; Frounfelker, B. D.; Cipriano, B. H.; Norman, A. I.; and Raghavan, S. R. Viscosity Increase with Temperature in Cationic Surfactant Solutions Due to the Growth of Wormlike Micelles. *Langmuir* **2005**, *21*, 10998-11004.

(24) Feng, Y.; Han Y. Effect of Counterion Size on Wormlike Micelles Formed by a C22-tailed Anionic Surfactant. *J. Mol. Liq.* **2016**, *218*, 508-514.

(25) Barhoum, S.; Castillob, R.; and Yethiraja A. Characterization of Dynamics and Internal Structure of a Mixed-surfactant Wormlike Micellar System Using NMR and Rheometry. *Soft Matter* **2012**, *8*, 6950–6957.

(26) Gallot, T.; Perge, C.; Grenard, V.; Fardin, M.-A.; Taberlet, N.; and Manneville, S. Ultrafast Ultrasonic Imaging Coupled to Rheometry: Principle and Illustration. *Rev. Sci. Instrum.* **2013**, *84*, 045107.

(27) Cardiel, J. J.; Zhao, Y.; de La Iglesia, P.; Pozzoc, L. D.; and Shen, A. Q. Turning Up the Heat on Wormlike Micelles with a Hydrotopic Salt in Microfluidics. *Soft Matter* **2014**, *10*, 9300–9312.

(28) Youssry, M.; Lemaire, E.; Caillard, B.; Colin, A.; and Dufour, I. On-chip Characterization of the Viscoelasticity of Complex Fluids Using Microcantilevers. *Meas. Sci. Technol.* **2012**, *23*, 125306.

(29) Cates, M. E. Reptation of Living Polymers: Dynamics of Entangled Polymers in the Presence of Reversible Chain-Scission Reactions. *Macromolecules* **1987**, *20*, 2289-2296.

(30) Turner, M. S.; and Cates, M. E. Linear Viscoelasticity of Living Polymers: A Quantitative Probe of Chemical Relaxation Times. *Langmuir* **1991**, *7*, 1590-1594.

(31) Khatory, A.; Lequeux, F.; Kern, F.; and Candau, S. J. Linear and Nonlinear Viscoelasticity of Semidilute Solutions of Wormlike Micelles at High Salt Content. *Langmuir* **1993**, 9, 1456-1464.

(32) Zou, W.; and Larson, R. G. A Mesoscopic Simulation Method for Predicting the Rheology of Semi-dilute Wormlike Micellar Solutions. *J. Rheol.* **2014**, *58*, 681-721.

(33) Zou, W.; Tang, X.; Weaver, M.; Koenig, P.; Larson, R. G. Determination of Characteristic Lengths and Times for Wormlike Micelle Solutions from Rheology Using a Mesoscopic Simulation Method. *J. Rheol.* **2015**, *59*, 903-934.

(34) Buchanan, M.; Ataknorrami, M.; Palierne, J. F.; and Schmidt, C. F. Comparing Macrorheology and One- and Two-point Microrheology in Wormlike Micelle Solutions. *Macromolecules* **2005**, *38*, 8840–8844.

(35) Oelschlaeger, C.; Schopferer, M.; Scheffold, F.; and Willenbacher, N. Linear-to-branched Micelles Transition: A Rheometry and Diffusing Wave Spectroscopy (DWS) Study. *Langmuir* **2009**, *25*, 716–723.

(36) Vogtt, K.; Beaucage, G.; Weaver, M.; and Jiang, H. Scattering Function for Branched Wormlike Chains. *Langmuir* **2015**, *31*, 8228−8234.

(37) Vogtt, K.; Jiang, H.; Beaucage, G.; and Weaver, M. Free Energy of Scission for Sodium Laureth-1-Sulfate Wormlike Micelles. *Langmuir* **2017**, *33*, 1872−1880.

(38) Shikata, T.; and Hirata, H.; Kotaka, T. Micelle Formation of Detergent Molecules in Aqueous Media. 2. Role of Free Salicylate Ions on Viscoelastic Properties of Aqueous Cetyltrimethylammonium Bromide-Sodium Salicylate Solutions. *Langmuir* **1988**, *4*, 354-359.

(39) Messager, R.; Ott, A.; Chatenay, D.; Urbach, W.; and Langevin, D. Are Giant Micelles Living Polymers? *Phys. Rev. Lett.* **1988**, *60*, 1410-1413.

(40) Yan, Z.; Dai, C.; Zhao, M.; and Sun, Y. Rheological Characterizations and Molecular Dynamics Simulations of Self-assembly in an Anionic/cationic Surfactant Mixture. *Soft Matter* **2016**, *12*, 6058—6066.

(41) Padding, J. T.; Briels, W. J.; Stukan, M. R.; and Boek, E. S. Review of Multi-scale Particulate Simulation of the Rheology of Wormlike Micellar Fluids. *Soft Matter* **2009**, *5*, 4367–4375.

(42) Acharya, D. P.; Sato, T.; Kaneko, M.; Singh, Y.; Kunieda, H. Effect of Added Poly(oxyethylene)dodecyl Ether on the Phase and Rheological Behavior of Wormlike Micelles in Aqueous SDS Solutions. *J. Phys. Chem. B* **2006**, *110*, 754–760.

(43) Aniansson, E. A. G.; and Wall, S. N. On the Kinetics of Step-Wise Micelle Association. *J. Phys. Chem.* **1974**, *78*, 1024-1030.

(44) Tang, X.; Zou, W.; Koenig, P. H.; McConaughy, S. D.; Weaver, M. R.; Eike, D. M.; Schmidt, M. J.; and Larson, R. G. Multiscale Modeling of the Effects of Salt and Perfume Raw Materials on the Rheological Properties of Commercial Threadlike Micellar Solutions. *J. Phys. Chem. B* **2017**, *121*, 2468−2485.

(45) Sarmiento-Gomez, E.; Lopez-Diaz, D.; and Castillo, R. Microrheology and Characteristic Lengths in Wormlike Micelles made of a Zwitterionic Surfactant and SDS in Brine. *J. Phys. Chem. B* **2010**, *114*, 12193–12202.

(46) Waton, G.; and Zana, R. Relaxation in Wormlike Micelle Solutions, in Giant Micelles; Properties and Application. *Surfactant Science Series*, Chap. 10, CRC Taylor & Francis group, Boca Raton, **2007**.

(47) Larson, R. G. The Structure and Rheology of Complex Fluids. *Oxford University Press*: New York, **1999**.

(48) Turner, M. S.; and Cates, M. E. Linear Viscoelasticity of Wormlike Micelles: A Comparison of Micellar Reaction Kinetics. *J. Phys.* **1992**, *2*, 503–519.

(49) Cates, M. E. Dynamics of Living Polymers and Flexible Surfactant Micelles: Scaling Laws for Dilution. *J. Phys. France* **1988**, *49*, 1593-1600.

(50) Rafati, A. A.; Safatian, F. Thermodynamic Studies of Inclusion Complex Between Cetyltrimethylammonium Bromide (CTAB) and β -cyclodextrin (β -CD) in Water/n-butanol Mixture, Using Potentiometric Technique. *Phys. Chem. Liq.* **2008**, *46*, 587−598.

(51) Morse, D. C. Viscoelasticity of Concentrated Isotropic Solutions of Semiflexible Polymers: 1. Model and Stress Tensor. *Macromolecules* **1998**, *31*, 7030–7043.

(52) Morse, D. C. Viscoelasticity of Concentrated Isotropic Solutions of Semiflexible Polymers: 2. Linear Response. *Macromolecules* **1998**, *31*, 7044–7067.

(53) Gittes, F.; and MacKintosh, F. C. Dynamic Shear Modulus of a Semiflexible Polymer Network. *Phys. Rev. E* **1998**, *58*, 1241–1244.

(54) Roitman, D. B.; and Zimm, B. H. An Elastic Hinge Model for Dynamics of Stiff Chains. I. Viscoelastic Properties. *J. Chem. Phys.* **1984**, *81*, 6333-6347.

(55) Carriere, C. J.; Amis, E. J.; Schrag, J. L.; and Ferry, J. D. Dilute-solution Dynamic Viscoelastic Properties of Schizophyllan Polysaccharide. *Macromolecules* **1985**, *18*, 2019-2023.

(56) Amis, E. J.; Carriere, C. J.; and Ferry, J. D.; and Veis, A. Effect of pH on Collagen Flexibility Determined From Dilute Solution Viscoelastic Measurements. *Int. J. Biol. Macromol.* **1985**, *7*, 130-134.

(57) de Gennes, P. G. Scaling Concepts in Polymer Physics. *Cornell University Press*, Ithaca, New York, **1979**.

(58) Porte, G.; Appell, J.; and Poggi, Y. Experimental Investigations on the Flexibility of Elongated Cetylpyridinium Bromide Micelles. *J. Phys. Chem.* **1980**, *84*, 3105-3110.

(59) Appell, J.; Porte, G.; and Poggi, Y. Quantitative Estimate of the Orientational Persistence Length of Flexible Elongated Micelles of Cetylpyridinium Bromide. *J. Colloid Interface Sci.* **1982**, *87*, 492-499.

(60) Chen, W.; Butler, P. D.; and Magid, L. J. Incorporating Intermicellar Interactions in the Fitting of SANS Data from Cationic Wormlike Micelles. *Langmuir* **2006**, *22*, 6539-6548.

(61) Friedman, B.; O'Shaughnessy, B. Kinetics of Intermolecular Reactions in Dilute Polymer Solutions and Unentangled Melts. *Macromolecules* **1993**, *26*, 5726-5739.

(62) O'Shaughnessy, B. From Mean Field to Diffusion-Controlled Kinetics: Concentration-Induced Transition in Reacting Polymer Solutions. *Phys. Rev. Lett.* **1993**, *71*, 3331-3334.

(63) O'Shaughnessy, B.; Yu, J. Rheology of Wormlike Micelles: Two Universality Classes. *Phys. Rev. Lett.* **1995**, *74*, 4329-4332.

(64) Kern, F.; Lemarechal, P.; Candau, S. J.; and Cates, M. E. Rheological Properties of Semidilute and Concentrated Aqueous Solutions of Cetyltrimethylammonium Bromide in the Presence of Potassium Bromide. *Langmuir* **1992**, *8*, 437-440.

(65) Ilgenfritz, G.; Schneider, R.; Grell, E.; Lewitzki, E.; and Ruf, H. Thermodynamic and Kinetic Study of the Sphere-to-Rod Transition in Nonionic Micelles: Aggregation and Stress Relaxation in $C_{14}E_8$ and $C_{16}E_8/H_2O$ Systems. *Langmuir* **2004**, *20*, 1620-1630.

(66) Larson, R. G. *The Structure and Rheology of Complex Fluids*. Oxford University Press: New York, **1999**.

(67) Gaudino, D.; Pasquino, R.; and Grizzuti, N. Adding Salt to a Surfactant Solution: Linear Rheological Response of the Resulting Morphologies. *J. Rheol.* **2015**, *59*, 1363-1375.

(68) Spenley, N. A.; Cates, M. E.; and McLeish T. C. B. Nonlinear Rheology of Wormlike Micelles. *Phys. Rev. Lett.* **1993**, *71*, 939-942.

(69) Vasquez, P. A.; McKinley, G. H.; Cook, L. P. A Network Scission Model for Wormlike Micellar Solutions I. Model Formulation and Viscometric Flow Predictions. *J. Non-Newtonian Fluid Mech.* **2007**, *144*, 122-139.

(70) Chandler, H. D. Activation Energy and Entropy for Viscosity of Wormlike Micelle Solutions. *J. Colloid Interface Sci.* **2013**, *409*, 98-103.

(71) Lutz-Bueno, V.; Kohlbrecher, J.; Fischer, P. Shear Thickening, Temporal Shear Oscillations, and Degradation of Dilute Equimolar CTAB/NaSal Wormlike Solutions. *Rheol Acta* **2013**, *52*, 297–312.

(72) Louhichi, A.; Jacob, A.; Bouteiller, L.; and Vlassopoulos, D. Humidity Affects the Viscoelastic Properties of Supramolecular Living Polymers. *J. Rheol.* **2017**, *61*, 1173-1182.

90x50mm (150 x 150 DPI)